J. Fluid Mech. (1999), *vol.* 393, *pp.* 215–240. Printed in the United Kingdom

Resonant acoustic frequencies of a tandem cascade. Part 1. Zero relative motion

By B. M. WOODLEY AND N. PEAKE

Department of Applied Mathematics and Theoretical Physics, University of Cambridge, Silver Street, Cambridge CB3 9EW, UK

(Received 30 January 1998 and in revised form 12 November 1998)

In this paper we study the acoustic scattering between two flat-plate cascades, with the aim of investigating the possible existence of trapped modes. In practical terms this question is related to the phenomenon of acoustic resonance in turbomachinery, whereby such resonant modes are excited to large amplitude by unsteady processes such as vortex shedding. We use the Wiener–Hopf technique to analyse the scattering of the various wave fields by the cascade blades, and by considering the fields between adjacent blades, as well as between the cascades, we are able to take full account of the genuinely finite blade chords. Analytic expressions for the various scattering matrices are derived, and an infinite-dimensional matrix equation is formed, which is then investigated numerically for singularity. One advantage of this formulation is that it allows the constituent parts of the system to be analysed individually, so that for instance the behaviour of the gap between the blade rows alone can be investigated by omitting the finite-chord terms in the equations. We demonstrate that the system exhibits two types of resonance, at a wide range of parameter values. First, there is a cut-on/cut-off resonance associated with the gap between the rows, and corresponding to modes propagating parallel to the front face of the cascades. Second, there is a resonance of the downstream row, akin to a Parker mode, driven at low frequencies by a vorticity wave produced by trapped duct modes in the upstream row, and at higher frequencies by radiation modes (and the vorticity wave) between the blade rows. The predictions for this second set of resonances are shown to be in excellent agreement with previous experimental data. The resonant frequencies are also seen to be real for this twin cascade system, indicating that the resonances correspond to genuine trapped modes. The analysis in this paper is completed with non-zero axial flow but with zero relative rotation between the cascades – in Part 2 (Woodley & Peake 1999) we will show how non-zero rotation of the upstream row can be included.

1. Introduction

The phenomenon of acoustic resonance in aeroengine compressors, in which unsteady forcing provided by vortex shedding locks into a natural resonant mode of the compressor to produce large-amplitude, potentially damaging, excitation has long been known to occur, particularly on engine tests when the system is being run at off-design conditions. In order to be able to predict these resonance, it is necessary as a first step to calculate both the vortex shedding frequencies of the blade rows and the natural resonant frequencies of the system; the former has been considered

previously by the authors (Woodley & Peake 1997*a*,*b*), and the latter is the subject of the current paper.

The problem of the acoustic resonance of a single blade row has received considerable attention. Pioneering work was completed by Parker (1966, 1967), who predicted numerically and verified experimentally the existence of trapped modes, 'Parker modes', in a single cascade of airfoils, and an extensive body of related experimental work has been completed subsequently (see Parker & Stoneman 1989 for a review). In addition, Koch (1983) has repeated Parker's analysis with non-zero mean flow. Related to this issue, there has also been considerable interest in the existence of water-wave trapping by rigid bodies (see Evans & Linton 1991), and of acoustic waves trapping by obstacles in ducts (Evans & Linton 1994; Evans, Levitin & Vassiliev 1994).

In a real compressor, the alternate rotating (rotor) and stationary (stator) blade rows are positioned close together, with separations typically less than the blade chord length. It therefore follows that although the isolated blade row resonances mentioned above can occur, it seems very likely that strong coupling between adjacent rotor and stator rows can lead to additional resonant states, with the interaction between the rows mediated either acoustically or via the wake shed from the rotor row impinging on the downstream stators. In this paper we therefore propose to address the question of the existence of trapped modes for a two blade row system, and thereby extend Parker's original analysis.

In our model we assume, as is often the case in real compressor stages, that the curvature of the duct passage is small, and hence we may 'unwrap' the blade rows into two-dimensional cascades (for an annulus with inner and outer radii r_1 and r_2 respectively, we require that $(r_2 - r_1)/r_1 \ll 1$). Furthermore, we shall suppose in the first instance that the 'rotor' row is in fact not rotating relative to the stator row, and this will not only allow our results to be compared closely with existing experimental data, which seems to be almost exclusively restricted to this non-rotating case, but will also allow the physical mechanisms causing the resonances to be clearly identified and studied. The extension to include relative rotation introduces considerable complexity into the problem, but the analysis will be presented here in such a way that this extension can be made in a natural way, and will be described in Part 2 (Woodley & Peake 1999). Also, we suppose here that the rotor and stator rows have equal blade numbers, and the extension to unequal blade numbers will be included in Part 2.

The overall system under consideration is shown in figure 1. The labels $A_n, B_n, C_n \ldots$ refer to the amplitudes of the various sets of waves which exist in the different regions of the system. We will suppose that the blades are aligned at zero incidence to the oncoming steady flow, so that the steady flow is uniform. In this non-rotating case it follows that the rotor and stator rows have equal stagger angles, although their chord lengths will be different. The radiation modes in the gap between the blade rows are coupled by the scattering from the leading and trailing edges of the blades, thus giving rise to a complicated mode interaction problem, which will be solved using the Wiener–Hopf technique. The analysis follows closely that of Peake (1993), who treated the forced problem of a single vorticity wave incident on the leading edge of a single finite-blade cascade, and we shall keep the same notation as far as possible here. Our aim here, however, is to find the resonant acoustic modes of the unforced system. We note that earlier studies of the cascade problem, such as Koch (1971) and references contained therein, have been made, and that the reflection and transmission matrices applied in this paper have therefore appeared, in different contexts and in differing forms, before.

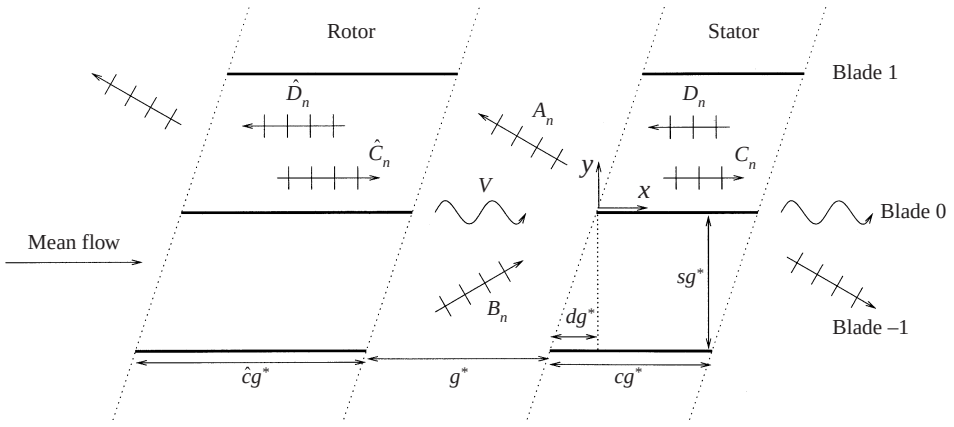

FIGURE 1. Twin finite-chord cascade system.

In view of the transverse periodicity of the system, we anticipate that the field in the gap between the blade rows will take the form of upstream- and downstream-travelling plane pressure (acoustic) waves, together with vorticity waves convected with the mean flow from the trailing edge of the upstream blade row so as to satisfy the unsteady Kutta condition there. Solution of the linearized Euler equations shows that these are the only two types of waves which are relevant; a third type of disturbance, entropy waves, does not lead to any fluctuations in the unsteady velocity field for uniform mean flow, and need not be considered here. In what follows we will non-dimensionalize all lengths by the blade-row gap g^*, velocities by the mean-flow speed U^*_∞ and densities by the undisturbed mean density ρ_∞. We use $\sigma_n^\pm$ to denote the x-wavenumbers of the pressure waves in the gap (full expressions will be given later, but we note here that the superfixes $^\pm$ relate to upstream and downstream propagating modes respectively), and Ω is the normalized frequency. For the purposes of our analysis, we let Ω have a small negative imaginary part (so that various Fourier integrals converge), which can be set to zero at the end of the calculation. The corresponding y-wavenumbers are calculated using the dispersion relation for sound waves in uniform compressible flow. Since the vorticity wave is convected with the mean flow its x-wavenumber is also Ω. The unsteady field can be described in terms of the velocity potential $\phi(x, y)$, with $\boldsymbol{u} = \mathrm{e}^{\mathrm{i}\Omega t}\nabla\phi$, and it follows, by summing over all the possible modes, that the unsteady field in the gap between the blade rows can be written in the form

$$\phi(x, y) = \sum_{n=-\infty}^{\infty} A_n \mathrm{e}^{-\mathrm{i}\sigma_n^+ x - \mathrm{i}\lambda_n^+ y} + \sum_{n=-\infty}^{\infty} B_n \mathrm{e}^{-\mathrm{i}\sigma_n^- x - \mathrm{i}\mu_n^- y} + V\mathrm{e}^{-\mathrm{i}\Omega x} f(y), \tag{1.1}$$

where the A_n and B_n are the (unknown) amplitudes of the upstream- and downstream-travelling pressure waves in the gap, and V is the (also unknown) vorticity wave amplitude. The function $f(y)$ in the vorticity wave amplitude can be simply obtained by substituting the final term in (1.1) into the convected wave equation. The quantities λ_n^+ and μ_n^- are the y-wavenumbers corresponding to the x-wavenumbers $\sigma_n^\pm$.

Our aim in this paper is to derive two sets of matrix equations relating the unknown amplitudes A_n,B_n and V, in the absence of any external forcing such as incident sound waves from upstream of the rotor row or downstream of the stator row. These matrix equations will then be analysed for the existence of non-trivial, resonant solutions. In

§2 we consider the scattering of the downstream-travelling pressure waves and the vorticity wave by the stator, and thereby determine expressions for the A_n in terms of the B_n and V. This calculation takes full account of the finite blade chord, which is accomplished by considering the repeated scattering by the stator leading and trailing edges, as in Peake (1993). In §3 the scattering of the upstream-travelling pressure waves is considered in much the same way, thereby yielding expressions for the B_n and V in terms of the A_n. In §4 the matching together of these two sets of results is described, and in §5 the numerical method used to search for resonance is outlined. In §6 full results are presented, and our predictions of resonant frequencies are seen to be in excellent agreement with previous experimental work on resonance in tandem blade rows. Broadly speaking, we identify two quite distinct types of resonance: one in which a pressure wave in the gap between the blade rows is close to its cut-off condition, and is therefore propagating in the transverse direction; and a second corresponding to resonance of the downstream blade row driven by the vorticity wave shed from the upstream blade row (this second resonance is akin to the original Parker modes, but unlike those is not restricted to having an inter-blade phase angle which is a multiple of π). A study of the effects of the various flow parameters on these resonances is also presented.

2. Stator scattering

In this section we consider the scattering of pressure and vorticity waves from upstream by the downstream (stator) blade row. We first analyse the initial scattering by the leading edges, assuming a semi-infinite blade chord, and then second consider the scattering of the resulting downstream-travelling duct modes between the blades by the trailing edges. The trailing-edge scattering produces upstream-travelling duct modes, which are in turn rescattered by the leading edges, and an infinite series of repeated reflection and rescattering is set up. We will proceed to use our results to derive a matrix equation relating the amplitudes of the duct modes in this infinite reflection series, and thereby derive exact expressions for the scattering by the blade row with a genuine finite chord.

2.1. *Leading edge*

We start by assuming that the stator blades are semi-infinite in the downstream direction, and solve for the scattering of incident pressure and vorticity waves by the leading edge. In effect we are thereby neglecting the effect of the upstream-travelling duct modes with amplitudes D_n (see figure 1), but these will be included in the next subsection. Since the system is periodic along the blade face, we concentrate on one blade passage, and use the periodic boundary conditions to calculate the field in the other blade passages.

Let $\phi_0(x, y)$ be the scattered field in the zeroth blade passage $0 < y < s$ due to the incidence of the downstream-travelling pressure and vorticity waves, with amplitudes B_n for $n = 0, \pm1, \pm2, \ldots$ and V respectively (i.e. the second and third terms in equation (1.1)), on the downstream blade row. By taking the half-range Fourier transform over $x > 0$ of the condition of total zero normal velocity on the zeroth blade, we obtain the equation

$$\frac{\partial \Phi_0^+}{\partial y}(k, 0) + \frac{\mathrm{i}V}{k - \Omega} + \sum_n \frac{\mu_n B_n}{k - \sigma_n^-} = 0, \tag{2.1}$$

where the superfix $^+$ indicates the transform over the positive semi-infinite x range.

In deriving (2.1) we have used the fact that the frequency Ω and wavenumbers σ_n^- possess negative imaginary parts, so that the various integrals converge, and in addition a factor $f'(0)$ has been absorbed into V. The scattered field must satisfy the convective wave equation, and taking the full-range Fourier transform in x of this equation yields

$$\frac{\partial^2 \Phi_0}{\partial y^2} + \gamma^2 \Phi_0 = 0, \tag{2.2}$$

where

$$\gamma^2(k;\Omega,M) = M^2\Omega^2 - 2kM^2\Omega - \beta^2 k^2 \tag{2.3}$$

and $\beta^2 = 1 - M^2$. The dispersion function $\gamma = \gamma(k;\Omega,M)$ is defined by taking branch cuts emanating from the points $k = -M\Omega/(1-M)$ and $k = M\Omega/(1+M)$ and going to infinity through the upper and lower half-planes respectively, and with $\gamma(0,\Omega,M) = +M\Omega$. We may then write down the general solution of (2.2) straightaway in the form

$$\Phi_0(k,y) = A\mathrm{e}^{-\mathrm{i}\gamma y} + B\mathrm{e}^{\mathrm{i}\gamma y}. \tag{2.4}$$

Owing to the transverse periodicity of the blade row geometry, it follows that the unsteady fields must satisfy the periodicity condition

$$\phi_N(x,y) = \phi_0(x - Nd, y - Ns)\,\mathrm{e}^{\mathrm{i}N\sigma}, \tag{2.5}$$

where ϕ_N is the field in the Nth blade passage $Ns < y < (N+1)s$, and σ is the prescribed inter-blade phase angle. (Here we note that although the phase angle is arbitrary for the purposes of this two-dimensional analysis, once we consider a genuine unwrapped blade row the phase angle will be restricted to the discrete values $\sigma = 2n\pi/N_B$ for some integer n, where N_B is the number of blades in the row, in order to ensure periodicity around the annulus.) We now use this periodicity condition, together with the condition that the scattered normal velocity must be continuous across $y = 0$ for all x, to show that

$$\Phi_0(k,y) = A\left(1 - \mathrm{e}^{-\mathrm{i}\sigma - \mathrm{i}kd - \mathrm{i}\gamma s}\right)\left[\frac{\mathrm{e}^{-\mathrm{i}\gamma y}}{1 - \mathrm{e}^{-\mathrm{i}\sigma - \mathrm{i}kd - \mathrm{i}\gamma s}} + \frac{\mathrm{e}^{\mathrm{i}\gamma y}}{1 - \mathrm{e}^{-\mathrm{i}\sigma - \mathrm{i}kd + \mathrm{i}\gamma s}}\right]. \tag{2.6}$$

We now turn our attention to the imposition of the condition of zero pressure jump across $y = 0$ for $x < 0$. By taking the full-range Fourier transform of the linearized Bernoulli relation between pressure and unsteady potential, and by applying the periodicity condition, we find a relation between the unknowns A and $[P(k,0)]_-^+$, the Fourier transform of the pressure jump across $x = 0$, leading to

$$\Phi_0(k,y) = \frac{[P(k,0)]_-^+}{2\mathrm{i}(k-\Omega)}\left[\frac{\mathrm{e}^{-\mathrm{i}\gamma y}}{1 - \mathrm{e}^{-\mathrm{i}\sigma - \mathrm{i}kd - \mathrm{i}\gamma s}} + \frac{\mathrm{e}^{\mathrm{i}\gamma y}}{1 - \mathrm{e}^{-\mathrm{i}\sigma - \mathrm{i}kd + \mathrm{i}\gamma s}}\right]. \tag{2.7}$$

We wish to find an expression for $[P(k,0)]_-^+$ in terms of the incident pressure and vorticity waves. The y-derivative of Φ_0 is written as a sum of parts analytic in the upper and lower halves of the complex k-plane as

$$\frac{\partial \Phi_0}{\partial y} = \frac{\partial \Phi_0^+}{\partial y} + \frac{\partial \Phi_0^-}{\partial y}, \tag{2.8}$$

where we now have an expression for the left-hand side from (2.7) above. Using (2.8),

and substituting for $\partial \Phi_0^+/\partial y$ in (2.1), we get

$$\frac{[P_0(k,0)]_-^+}{\mathscr{K}(k)} - \frac{\partial \Phi_0^-}{\partial y} + \frac{\mathrm{i}V}{k-\Omega} + \sum_n \frac{\mu_n^- B_n}{k-\sigma_n^-} = 0, \tag{2.9}$$

where the Wiener–Hopf kernel function $\mathscr{K}(k)$ is given by

$$\mathscr{K}(k) = -\frac{2\mathrm{i}(k-\Omega)}{\gamma \sin(\gamma s)} [\cos(\sigma + kd) - \cos(\gamma s)]. \tag{2.10}$$

The kernel $\mathscr{K}(k)$ is factorized into a product of functions analytic and non-zero in the upper and lower half-planes, as

$$\mathscr{K}(k) = \mathscr{K}^+(k)\mathscr{K}^-(k). \tag{2.11}$$

On multiplying (2.9) through by $\mathscr{K}^-(k)$ and performing an additive factorization of two terms of the form $\mathscr{K}^-(k)/(k-v)$ for v in the lower half of the k-plane, we obtain an equation of the form $F^+(k) = F^-(k)$, with the left- and right-hand sides analytic in the upper and lower half-planes respectively. By analytically continuing these functions we may define a function, $F(k)$, which is analytic over the whole of the complex k-plane, and it can then be shown that, due to the incompressibility of the flow in the neighbourhood of the leading edge, $F(k)$ decays algebraically to zero as $k \to \infty$, and hence by Liouville's Theorem that $F(k) = 0$ for all k. This then yields an expression for the previously unknown $[P_0(k,0)]_-^+$, and substituting in (2.7) we obtain an expression for the Fourier-transformed velocity potential as

$$\Phi_0(k,y) = \frac{\mathscr{K}^+(k)}{2\mathrm{i}(k-\Omega)} \left[-\frac{\mathrm{i}V\mathscr{K}^-(\Omega)}{k-\Omega} - \sum_n \frac{\mu_n^- B_n \mathscr{K}^-(\sigma_n^-)}{k-\sigma_n^-} \right] \times \left[\frac{\mathrm{e}^{-\mathrm{i}\gamma y}}{1-\mathrm{e}^{-\mathrm{i}\sigma - \mathrm{i}kd - \mathrm{i}\gamma s}} + \frac{\mathrm{e}^{\mathrm{i}\gamma y}}{1-\mathrm{e}^{-\mathrm{i}\sigma - \mathrm{i}kd + \mathrm{i}\gamma s}} \right]. \tag{2.12}$$

The factorization of $\mathscr{K}(k)$ may be carried out using infinite products, as described in Peake (1993). This decomposition can be computed in a very efficient way using Richardson extrapolation, as described by Majumdar & Peake (1996), and this approach will be applied here as well.

We may now proceed to invert the spatial Fourier transform in order to determine the scattered field $\phi_0(x,y)$. The zeros of $\mathscr{K}(k)$ (and hence the poles of $\Phi_0(k,y)$) lie at $k = \sigma_n^\pm$ for $n = 0, \pm 1, \pm 2, \ldots$ in the upper and lower half-planes respectively, and satisfy

$$\gamma(\sigma_n^\pm)s = \pm(2n\pi - \sigma - \sigma_n^\pm d) \tag{2.13}$$

(unrelated plus and minus signs), leading to

$$\sigma_n^\pm = \frac{d(2n\pi - \sigma) - M^2\Omega s^2 \mp \mathscr{S}}{d^2 + s^2\beta^2} \tag{2.14}$$

where

$$\mathscr{S}^2 = [s^2(d^2+s^2)M^2\Omega^2 - 2dM^2\Omega s^2(2n\pi - \sigma) - s^2\beta^2(2n\pi - \sigma)^2]^{1/2}, \tag{2.15}$$

and $\mathscr{S} = |\mathscr{S}|$ when $\mathscr{S}^2 > 0$ and $\mathscr{S} = -\mathrm{i}|\mathscr{S}|$ when $\mathscr{S}^2 < 0$. The fact that Ω possesses a negative imaginary part leads to $\sigma_n^\pm$ being situated in the upper and lower halves of the complex k-plane. However, we emphasize that the superfix $\pm$ on $\sigma_n^\pm$ is unrelated to the $\pm$ on the right-hand side of (2.13). For $x < 0$ we must close the inversion

contour in the upper half-plane. The residue of the term in the second square brackets in (2.12) at $k = \sigma_n^+$ is then given by

$$Res^1_{\sigma_n^+}(y) = -\frac{\gamma(\sigma_n^+)}{\gamma(\sigma_n^+)d\sin(\sigma+\sigma_n^+ d) + s(M^2\Omega + \beta^2\sigma_n^+)\sin\gamma(\sigma_n^+)s}$$
$$\times[\tfrac{1}{2}(\mathrm{e}^{\mathrm{i}\sigma+\mathrm{i}\sigma_n^+ d} - \mathrm{e}^{-\mathrm{i}\gamma(\sigma_n^+)s})\mathrm{e}^{-\mathrm{i}\gamma(\sigma_n^+)y} + \tfrac{1}{2}(\mathrm{e}^{\mathrm{i}\sigma+\mathrm{i}\sigma_n^+ d} - \mathrm{e}^{\mathrm{i}\gamma(\sigma_n^+)s})e^{\mathrm{i}\gamma(\sigma_n^+)y}], \tag{2.16}$$

where one of the terms in these square brackets must necessarily be zero, depending on which sign is satisfied by $\gamma(\sigma_n^+)$ in (2.13).

By comparing the results of this calculation with the expression for the field in the gap between the blade rows given in (1.1), we may equate coefficients of $\exp(-\mathrm{i}\sigma_n^+ x)$, giving an equation for the coefficients of left-travelling radiation modes, A_n, in the form

$$A_n = \frac{\mathscr{K}^+(\sigma_n^+)}{2(\sigma_n^+ - \Omega)} \times Res^1_{\sigma_n^+}(0) \times \left[-\frac{\mathrm{i}V\mathscr{K}^-(\Omega)}{\sigma_n^+ - \Omega} - \sum_m \frac{\mu_m^- B_m \mathscr{K}^-(\sigma_m^-)}{(\sigma_n^+ - \sigma_m^-)}\right]. \tag{2.17}$$

Note that the y-wavenumber μ_n^+ in (1.1) is equivalent to either $\pm\gamma(\sigma_n^+)$, again depending upon which sign in (2.13) is satisfied by that particular pressure mode.

We have thus determined the amplitudes A_n in terms of the unknown B_n and V, and at this stage we write down the coupling coefficients between the nth reflected pressure wave and the mth incident pressure wave in the form

$$T_{mn}^{\mathscr{P}\mathscr{P}} = -\frac{\mathscr{K}^+(\sigma_n^+)}{2(\sigma_n^+ - \Omega)} \times Res^1_{\sigma_n^+}(0) \times \frac{\mu_m{}^- \mathscr{K}^-(\sigma_m^-)}{(\sigma_n^+ - \sigma_m^-)}, \tag{2.18}$$

and the coupling coefficient between the nth reflected pressure wave and the incident vorticity wave in the form

$$T_n^{\mathscr{V}\mathscr{P}} = -\frac{\mathscr{K}^+(\sigma_n^+)}{2(\sigma_n^+ - \Omega)} \times Res^1_{\sigma_n^+}(0) \times \frac{\hat{\mathscr{K}}^-(\Omega)}{(\sigma_n^+ - \Omega)}. \tag{2.19}$$

In the next subsection we extend these results to account for the finite stator blade chord.

2.2. *Trailing edge*

In this subsection we will include the effects of the scattering of the duct modes by the stator blade leading and trailing edges, and thereby extend the results in the previous section to account for the genuine finite blade chord. The duct-mode field in the stator blade passages may be obtained simply by solving the convective wave equation with hard-wall boundary conditions, and may be taken straight from Peake (1993) as

$$\phi_0 = \sum_{n=0}^{\infty} C_n \mathrm{e}^{\mathrm{i}k_n^- d}\cos\left(\frac{n\pi y}{s}\right)\mathrm{e}^{-\mathrm{i}k_n^- x} + \sum_{n=0}^{\infty} D_n \mathrm{e}^{\mathrm{i}k_n^+ c}\cos\left(\frac{n\pi y}{s}\right)\mathrm{e}^{-\mathrm{i}k_n^+ x}, \tag{2.20}$$

where the x-wavenumbers are

$$k_n^{\pm} = \frac{-M^2\Omega \mp \mathscr{T}}{1 - M^2}, \tag{2.21}$$

where

$$\mathscr{T}^2 = M^2\Omega^2 - (1 - M^2)\frac{n^2\pi^2}{s^2}, \tag{2.22}$$

with $\mathscr{T} = |\mathscr{T}|$ when $\mathscr{T}^2 > 0$ and $\mathscr{T} = -\mathrm{i}|\mathscr{T}|$ when $\mathscr{T}^2 < 0$. In (2.21) the distorted vorticity wave, which does not contribute to the noise generation at the trailing edge, has been omitted. The quantities $k_n^{\pm}$ are the wavenumbers of the upstream- and downstream-propagating duct modes respectively. The $\exp(\mathrm{i}k_n^- d)$ and $\exp(\mathrm{i}k_n^+ c)$ terms in (2.21) are included to ensure that the amplitude coefficients decay algebraically as $n \to \infty$. We may now write down a formal expression for the radiation field reflected back upstream from the stator as

$$A_m = \sum_p T_{pm}^{\mathscr{P}\mathscr{P}} B_p + T_m^{\mathscr{V}\mathscr{P}} V + \sum_p T_{pm}^{\mathscr{D}\mathscr{P}} D_p, \tag{2.23}$$

where the coupling matrices $\boldsymbol{T}^{\mathscr{P}\mathscr{P}}$ and $\boldsymbol{T}^{\mathscr{V}\mathscr{P}}$ have already been calculated in the previous subsection, and represent the generation of reflected pressure waves by the scattering of incident pressure waves and vorticity waves from upstream, and the as yet unknown coupling matrix $\boldsymbol{T}^{\mathscr{D}\mathscr{P}}$ represents the scattering of upstream-travelling duct modes at the stator leading edges.

Since we are supposing that there is no upstream-travelling radiation incident on the stator trailing edge from downstream, it follows that the amplitudes of the upstream-travelling duct modes, C_m, can be related to the amplitudes of the downstream-travelling duct modes, D_m, by the expression

$$D_m = \sum_p R_{pm}^{\mathscr{D}\mathscr{D}} C_p, \tag{2.24}$$

for some reflection matrix $\boldsymbol{R}^{\mathscr{D}\mathscr{D}}$. This reflection matrix can be calculated by considering the trailing-edge scattering, in much the same way as in the previous subsection, and is given in Appendix A. The amplitudes C_m are themselves determined from the incidence of the pressure waves, vorticity waves and upstream-travelling duct modes on the leading edges of the stator cascade, and can be expressed in the form

$$C_m = \sum_p T_{pm}^{\mathscr{P}\mathscr{D}} B_p + T_m^{\mathscr{V}\mathscr{D}} V + \sum_p T_{pm}^{\mathscr{D}\mathscr{D}} D_p. \tag{2.25}$$

Here, the coupling matrices $\boldsymbol{T}^{\mathscr{P}\mathscr{D}}$ and $\boldsymbol{T}^{\mathscr{V}\mathscr{D}}$ represent the scattering of the incident upstream pressure and vorticity waves into downstream-travelling duct modes, and $\boldsymbol{T}^{\mathscr{D}\mathscr{D}}$ represents the scattering of upstream-travelling duct modes into downstream-travelling duct modes at the leading edges. Again, these matrices can be determined in much the same way as in the previous subsection, and full expressions are given in Appendix A.

We now eliminate the C_m by substituting (2.25) into (2.24), and hence express D_m in terms of the incident pressure and vorticity waves, and find that

$$\sum_{r=0}^{\infty} S_{pr} D_r = \sum_{q=0}^{\infty} R_{qp}^{\mathscr{D}\mathscr{D}} \left[T_q^{\mathscr{V}\mathscr{D}} V + \sum_{r=-\infty}^{\infty} T_{rq}^{\mathscr{P}\mathscr{D}} B_r \right], \tag{2.26}$$

where

$$S_{pr} = \delta_{pr} - \sum_{q=0}^{\infty} R_{qp}^{\mathscr{D}\mathscr{D}} T_{rq}^{\mathscr{D}\mathscr{D}}. \tag{2.27}$$

Equation (2.26) above is now just a simple matrix equation for the vector $\boldsymbol{D}$, and if

$[S^{-1}]_{pr}$ is the left inverse of S_{pr} it follows that

$$D_m = \sum_{p=0}^{\infty} [S^{-1}]_{pm} \sum_{q=0}^{\infty} R_{qp}^{\mathscr{D}\mathscr{D}} \left[T_q^{\mathscr{V}\mathscr{D}} V + \sum_{r=-\infty}^{\infty} T_{qr}^{\mathscr{P}\mathscr{D}} B_r \right]. \tag{2.28}$$

Finally, by substituting $\boldsymbol{D}$ back into the right-hand side of (2.23), we find that the amplitudes of the upstream-propagating pressure waves generated by the scattering of incident downstream-propagating pressure and vorticity waves are given by

$$A_m = T_m^{\mathscr{V}} V + \sum_r T_{rm}^{\mathscr{P}} B_r, \tag{2.29}$$

where

$$T_{rm}^{\mathscr{P}} = T_{rm}^{\mathscr{P}\mathscr{P}} + T_{rm}^{\mathscr{P}\mathscr{D}\mathscr{P}}, \quad T_m^{\mathscr{V}} = T_m^{\mathscr{V}\mathscr{P}} + T_m^{\mathscr{V}\mathscr{D}\mathscr{P}}, \tag{2.30}$$

with

$$T_{rm}^{\mathscr{P}\mathscr{D}\mathscr{P}} = \sum_{p=0}^{\infty} T_{pm}^{\mathscr{D}\mathscr{P}} \sum_{s=0}^{\infty} [S^{-1}]_{sp} \sum_{q=0}^{\infty} R_{qs}^{\mathscr{D}\mathscr{D}} T_{qr}^{\mathscr{P}\mathscr{D}}, \tag{2.31}$$

and

$$T_m^{\mathscr{V}\mathscr{D}\mathscr{P}} = \sum_{p=0}^{\infty} T_{pm}^{\mathscr{D}\mathscr{P}} \sum_{s=0}^{\infty} [S^{-1}]_{sp} \sum_{q=0}^{\infty} R_{qs}^{\mathscr{D}\mathscr{D}} T_q^{\mathscr{V}\mathscr{D}}. \tag{2.32}$$

From (2.29) we see that $\boldsymbol{T}^{\mathscr{P}\mathscr{P}}$ and $\boldsymbol{T}^{\mathscr{V}\mathscr{P}}$ represent the contribution to the reflected pressure waves from the direct scattering of incident pressure and vorticity waves from upstream (as found in § 2.1), while $\boldsymbol{T}^{\mathscr{P}\mathscr{D}\mathscr{P}}$ represents the indirect scattering of incident pressure waves into reflected pressure waves via the multiply-reflected duct modes wave, and $\boldsymbol{T}^{\mathscr{V}\mathscr{D}\mathscr{P}}$ represents the indirect scattering of incident vorticity waves into reflected pressure waves via the duct modes. It therefore follows that $\boldsymbol{T}^{\mathscr{P}\mathscr{D}\mathscr{P}}$ and $\boldsymbol{T}^{\mathscr{V}\mathscr{D}\mathscr{P}}$ represent the corrections to the results derived in § 2.1 to account for the finite blade chord.

3. Rotor scattering

In this section we will consider the scattering of the pressure waves which propagate upstream in the blade-row gap by the rotors. We first consider the scattering by the trailing edges alone with the rotor blades assumed to have a semi-infinite chord, and then in § 3.2 include the effect of finite chord by considering the repeated reflections and rescattering of the duct-mode field by the rotor-blade leading and trailing edges. The analysis proceeds in much the same way as the stator calculations in the previous section, and we therefore need give only the broadest outline of the method here.

3.1. *Trailing edge*

Let $\hat{\phi}_0$ now be the scattered field due to the incidence of the upstream-travelling pressure waves, amplitudes $\hat{A}_n$ $n = 0, \pm 1, \pm 2, \ldots$, on the trailing edge of the upstream blade row, where we use $\hat{}$ to denote rotor variables (the amplitudes $\hat{A}_n$ differ from the amplitudes A_n in equation (1.1) by a simple phase shift arising from a change of origin). The system is shown in figure 2, and we introduce the rotor-shifted coordinates $\hat{x} = x + 1$, $\hat{y} = y$. We must now apply the condition of zero total normal velocity on the zeroth rotor blade $\hat{y} = 0$, $\hat{x} < 0$, with the scattered field satisfying the periodicity condition (2.5), and with the unsteady pressure being continuous across the blade

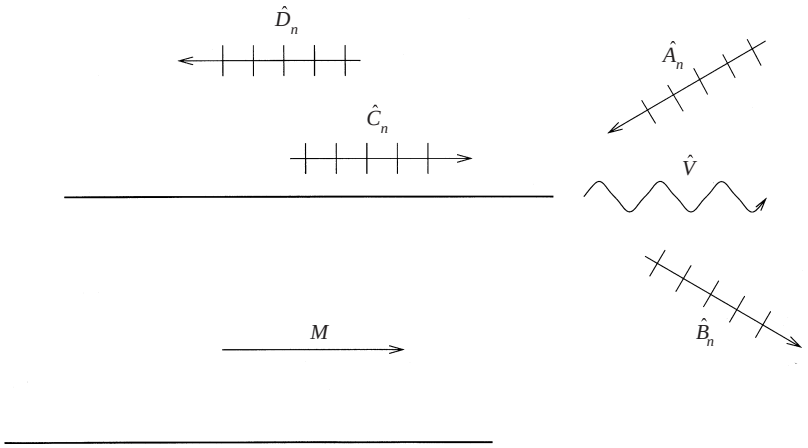

FIGURE 2. Rotor duct geometry and wave fields.

wake $\hat{y} = 0$, $\hat{x} > 0$. An additional feature not present in § 2.1 is that now an unsteady Kutta condition of zero pressure jump at the trailing edge must be enforced.

The problem is again solved using the Wiener–Hopf technique, in much the same way as in § 2 and as in Peake (1993), and we will therefore present just the results of the analysis here. First, the Wiener–Hopf equation leads to an expression for the Fourier transform of the unsteady pressure jump across the zeroth rotor blade in the form

$$\frac{[\hat{P}_0(k,0)]^+_-}{\mathscr{K}^-(k)} - \sum_n \frac{\lambda_n^+ \hat{A}_n \mathrm{e}^{\mathrm{i}\sigma_n^+} \mathscr{K}^+(\sigma_n^+)}{k - \sigma_n^+} = 0, \tag{3.1}$$

where now k is the transform variable corresponding to $\hat{x}$. Second, it follows from this that the solution for the transform of the unsteady potential in $0 < \hat{y} < s$ is

$$\hat{\Phi}_0(k,\hat{y}) = \frac{\mathscr{K}^-(k)}{2\mathrm{i}(k-\Omega)} \left[\sum_n \frac{\lambda_n^+ \hat{A}_n \mathrm{e}^{\mathrm{i}\sigma_n^+} \mathscr{K}^+(\sigma_n^+)}{k - \sigma_n^+} \right] \times \left[\frac{\mathrm{e}^{-\mathrm{i}\gamma\hat{y}}}{1 - \mathrm{e}^{-\mathrm{i}\sigma - \mathrm{i}kd - \mathrm{i}\gamma s}} + \frac{\mathrm{e}^{\mathrm{i}\gamma\hat{y}}}{1 - \mathrm{e}^{-\mathrm{i}\sigma - \mathrm{i}kd + \mathrm{i}\gamma s}} \right]. \tag{3.2}$$

The field scattered back into the gap can now be determined by inverting this transform and closing the contour in the lower half of the k-plane. It is clear from (3.2) that the transform possesses a pole at $k = \Omega$, which will correspond to the vorticity wave shed from the rotor trailing edge. The amplitude of this vorticity wave is related to the amplitudes of the incident pressure waves via a coupling matrix $\hat{T}_m^{\mathscr{P}\mathscr{V}}$, with the amplitude of the vorticity wave being

$$\sum_n \hat{T}_n^{\mathscr{P}\mathscr{V}} A_n. \tag{3.3}$$

Using the residue theorem, it is easy to show from (3.2) that

$$\hat{T}_m^{\mathscr{P}\mathscr{V}} = -\frac{\mathrm{e}^{\mathrm{i}(\sigma_m^+ - \Omega)} \mathscr{K}^-(\Omega) \lambda_m^+ \mathscr{K}^+(\sigma_m^+)}{2(\Omega - \sigma_m^+)} \left[1 + \frac{\mathrm{i}\sin(\sigma + \Omega d)}{\cos(\sigma + \Omega d) - \cos(\gamma(\Omega) s)} \right]. \tag{3.4}$$

Furthermore, it also follows that the transform in (3.2) possesses poles at $k = \sigma_n^-$ $n = 0, \pm 1, \pm 2, \ldots$, which correspond to the downstream-propagating pressure waves in the gap between the blade rows. Again, the amplitudes of these scattered pressure waves in terms of the amplitudes of the incident pressure waves can be expressed in terms of the coupling matrix $\hat{T}_{pm}^{\mathscr{P}\mathscr{P}}$; the amplitude of downstream pressure mode n is

$$\hat{B}_n = \sum_m \hat{T}_{nm}^{\mathscr{P}\mathscr{P}} \hat{A}_m, \tag{3.5}$$

and it can be shown by again applying the residue theorem to (3.2) that

$$\hat{T}_{nm}^{\mathscr{P}\mathscr{P}} = -\frac{e^{i(\sigma_m^+ - \sigma_n^-)} \mathscr{K}^-(\sigma_n^-)}{2(\sigma_n^- - \Omega)} \times Res_{\sigma_n^-}^2 \times \frac{\lambda_m^+ \mathscr{K}^+(\sigma_n^+)}{(\sigma_n^- - \sigma_m^+)}, \tag{3.6}$$

where

$$Res_{\sigma_n^-}^2 = -\frac{\gamma(\sigma_n^-)}{\gamma(\sigma_n^-) d \sin(\sigma + \sigma_n^- d) + s(M^2\Omega + \beta^2 \sigma_n^-) \sin \gamma(\sigma_n^-) s} \times [\tfrac{1}{2}(e^{i\sigma + i\sigma_n^- d} - e^{-i\gamma(\sigma_n^-)s}) + \tfrac{1}{2}(e^{i\sigma + i\sigma_n^- d} - e^{i\gamma(\sigma_n^-)s})]. \tag{3.7}$$

As in § 2, one of the terms in square brackets in (3.8) will be zero, depending on the precise value of $\gamma(\sigma_n^-)$.

3.2. *Leading edge*

Here we describe the corrections to the semi-infinite rotor cascade model, in very similar terms to that for the finite-chord stator corrections of § 2.2. From figure 2 we may immediately write down four equations defining the wave scattering by the rotor with only pressure waves incident from downstream, and no incoming waves from upstream.

In the notation of the figure,

$$\hat{B}_m = \sum_{p=-\infty}^{\infty} \hat{T}_{pm}^{\mathscr{P}\mathscr{P}} \hat{A}_p + \sum_{p=0}^{\infty} \hat{T}_{pm}^{\mathscr{D}\mathscr{P}} \hat{C}_p, \tag{3.8}$$

$$\hat{V}_n = \sum_{m=-\infty}^{\infty} \hat{T}_m^{\mathscr{P}\mathscr{V}} \hat{A}_m + \sum_{m=0}^{\infty} \hat{T}_m^{\mathscr{D}\mathscr{V}} \hat{C}_m, \tag{3.9}$$

$$\hat{D}_m = \sum_{p=-\infty}^{\infty} \hat{T}_{pm}^{\mathscr{P}\mathscr{D}} \hat{A}_p + \sum_{p=0}^{\infty} \hat{R}_{pm}^{\mathscr{D}\mathscr{D}} \hat{C}_p, \tag{3.10}$$

$$\hat{C}_m = \sum_{p=0}^{\infty} \hat{T}_{pm}^{\mathscr{D}\mathscr{D}} \hat{D}_p. \tag{3.11}$$

Here, the coupling matrices $\hat{T}_m^{\mathscr{P}\mathscr{V}}$ and $\hat{T}_{nm}^{\mathscr{P}\mathscr{P}}$, describing the direct scattering of upstream-travelling pressure waves into downstream-travelling vorticity and pressure waves, have already been derived in the previous subsection. The remaining matrices describe the way in which the duct modes in the rotor blade passages are scattered; $\hat{T}_m^{\mathscr{D}\mathscr{V}}$ is the coupling matrix for scattering of the mth downstream-travelling duct modes into the vorticity wave, and $\hat{T}_{pm}^{\mathscr{D}\mathscr{P}}$ corresponds to scattering of the pth duct mode into the mth downstream-propagating pressure wave. The amplitudes of the duct modes themselves are expressed using (3.10) and (3.11); $\hat{T}_{pm}^{\mathscr{P}\mathscr{D}}$ describes the

scattering of the pth upstream radiation mode into the mth upstream travelling duct mode, $\hat{R}^{\mathscr{D}\mathscr{D}}_{pm}$ corresponds to the reflection of the pth downstream-travelling duct mode into the mth upstream-travelling duct mode at the rotor trailing edges, and the matrix $\hat{T}^{\mathscr{D}\mathscr{D}}_{pm}$ describes the coupling of upstream- and downstream-travelling duct modes at the rotor leading edges. Expressions for all these matrices are given in Appendix B.

As was done for the finite-chord stator corrections, we may simply substitute equation (3.10) into equation (3.11) and invert the left-hand side to give the expression

$$\hat{C}_m = \sum_{r=0}^{\infty} [\hat{S}^{-1}]_{rm} \sum_{p=0}^{\infty} \hat{T}^{\mathscr{D}\mathscr{D}}_{pr} \sum_{q=-\infty}^{\infty} \hat{T}^{\mathscr{P}\mathscr{D}}_{pq} \hat{A}_q, \tag{3.12}$$

where

$$\hat{S}_{qm} = \delta_{mq} - \sum_{p=0}^{\infty} \hat{T}^{\mathscr{D}\mathscr{D}}_{pm} \hat{R}^{\mathscr{D}\mathscr{D}}_{qp}. \tag{3.13}$$

This may then be substituted into equations (3.8) and (3.9) to give the correction matrices $\hat{\boldsymbol{T}}^{\mathscr{P}\mathscr{D}\mathscr{P}}$ and $\hat{\boldsymbol{T}}^{\mathscr{P}\mathscr{D}\mathscr{V}}$, in the forms

$$\hat{T}^{\mathscr{P}\mathscr{D}\mathscr{P}}_{pm} = \sum_{r=0}^{\infty} \hat{T}^{\mathscr{D}\mathscr{P}}_{rm} \hat{X}_{rp}, \tag{3.14}$$

$$\hat{T}^{\mathscr{P}\mathscr{D}\mathscr{V}}_{m} = \sum_{r=0}^{\infty} \hat{T}^{\mathscr{D}\mathscr{V}}_{r} \hat{X}_{rm}, \tag{3.15}$$

where

$$\hat{X}_{pr} = \sum_{s=0}^{\infty} \sum_{q=0}^{\infty} [\hat{S}^{-1}]_{sp} \hat{T}^{\mathscr{D}\mathscr{D}}_{qs} \hat{T}^{\mathscr{P}\mathscr{D}}_{qr}. \tag{3.16}$$

We may now write down the corrected reflection matrices in forms similar to those for the stator as

$$\hat{T}^{\mathscr{P}}_{pm} = \hat{T}^{\mathscr{P}\mathscr{P}}_{pm} + \hat{T}^{\mathscr{P}\mathscr{D}\mathscr{P}}_{pm}, \tag{3.17}$$

and

$$\hat{T}^{\mathscr{V}}_{m} = \hat{T}^{\mathscr{P}\mathscr{V}}_{m} + \hat{T}^{\mathscr{P}\mathscr{D}\mathscr{V}}_{m}. \tag{3.18}$$

Just as in (2.30), the first terms on the right-hand side correspond to the direct scattering by the rotor trailing edges, and the second terms correspond to the corrections to account for the finite rotor chord.

The analysis of the stationary twin cascade problem with finite-chord blades has now been completed. We must next match the two wave fields across the inter-row gap in order to find an overall matrix equation for the amplitude coefficients. In Part 2 we will describe how to include the effects of non-zero rotation on the rotor.

4. Rotor–stator matching

We now have an infinite system of linear equations for the amplitude vectors $\boldsymbol{A}$, $\boldsymbol{B}$ (coefficients A_n and B_n $n = 0, \pm1, \pm2, \ldots$ respectively), and the vorticity wave amplitude V, of the form

$$A_n = T^{\mathscr{V}}_{n} V + \sum_{m} T^{\mathscr{P}}_{nm} B_m, \tag{4.1}$$

$$B_n = \sum_m \hat{T}^{\mathscr{P}}_{nm} A_m, \tag{4.2}$$

$$V = \sum_n \hat{T}^{\mathscr{V}}_n A_n, \tag{4.3}$$

where the summations run from $-\infty$ to $+\infty$. Expressions for all these matrices have been derived in the previous sections.

It may be shown that the m–n elements of $T^{\mathscr{P}}_{nm}$ and $\hat{T}^{\mathscr{P}}_{nm}$ and the n elements of $T^{\mathscr{V}}_n$ and $\hat{T}^{\mathscr{V}}_n$ decay exponentially as $m, n \to \infty$, and so we may truncate the infinite summations at some finite value, N say, and solve the resulting finite matrix system. For convenience, we group the single V-term together with the $\boldsymbol{B}$ vector to form a new vector $\boldsymbol{B}'$, and we may thus write

$$A_n = \sum_{m=-N}^{N+1} T'_{nm} B'_m, \tag{4.4}$$

$$B'_n = \sum_{m=-N}^{N} \hat{T}'_{nm} A_m, \tag{4.5}$$

where now $B'_n = B_n$ for $n = -N \ldots N$, $B'_{N+1} = V$ and the $\boldsymbol{A}$ vector is unchanged. The new coupling matrices are now non-square and include a row for the vorticity wave interaction:

$$T'_{nm} = T^{\mathscr{P}}_{nm}, \tag{4.6}$$

$$\hat{T}'_{nm} = \hat{T}^{\mathscr{P}}_{nm}, \tag{4.7}$$

for $n, m = -N \ldots N$, and

$$T'_{n,N+1} = T^{\mathscr{V}}_n, \tag{4.8}$$

$$\hat{T}'_{N+1,m} = \hat{T}^{\mathscr{V}}_m. \tag{4.9}$$

We now have a system of linear equations for the amplitude vectors $\boldsymbol{A}'$ and $\boldsymbol{B}'$, and in particular we have the matrix equation

$$A_p = \sum_{m=-N}^{N+1} T'_{pm} \sum_{q=-N}^{N} \hat{T}'_{mq} A_q. \tag{4.10}$$

This can be expressed more clearly in the schematic form

$$\left(\begin{bmatrix} & \cdots & \\ \vdots & \boldsymbol{I} & \vdots \\ & \cdots & \end{bmatrix} - \begin{bmatrix} & \cdots & \cdots & \\ \vdots & \boldsymbol{T} & \ddots & \vdots \\ & \cdots & \cdots & \end{bmatrix} \begin{bmatrix} & \cdots & \\ \vdots & \hat{\boldsymbol{T}} & \vdots \\ \vdots & \vdots & \vdots \\ & \cdots & \end{bmatrix} \right) \begin{bmatrix} \vdots \\ \boldsymbol{A} \\ \vdots \end{bmatrix} = 0, \tag{4.11}$$

where the asymmetric nature of the matrices arising from the inclusion of the vorticity wave term becomes apparent. Defining a new matrix, $\boldsymbol{Q} = \boldsymbol{I} - \boldsymbol{T} \cdot \hat{\boldsymbol{T}}$, we may write the whole system as

$$\sum_q Q_{pq} A_q = 0, \tag{4.12}$$

where

$$Q_{pq} = \delta_{pq} - \sum_m T'_{pm} \hat{T}'_{mq}. \tag{4.13}$$

We have thus defined a matrix equation for the unknown amplitude coefficients A_n. In order to find a non-zero solution for this amplitude vector, and thus guarantee by linearity a non-zero solution for the B_n, we simply need to find values of the reduced frequency, Ω, such that the determinant of the matrix $\boldsymbol{Q}$ is zero, thus giving the resonance points at which a non-zero acoustic field may exist. The method used to determine such points and the results are described in the following sections.

5. Numerical methods

In this section we describe briefly the numerical techniques employed for determining the resonant modes of our system.

We first truncated the infinite-dimensional matrix equations to finite extent, as described in the previous sections. Inclusion of all the cut-on modes and a limited number of the cut-off ones would seem to be the best method here, and preliminary investigation revealed that a truncation number of $N = 4$ was sufficient for most cases.

Calculation of these resonance points for a wide range of parameters revealed resonances only for nearly *real* values of Ω. Of course it should be remembered that, mathematically, Ω must have a small negative imaginary part, so that the Fourier transform integrals converge at infinity. Likewise it is convenient to retain this small imaginary part for the numerical solution, so that we may distinguish the $\sigma_n^{\pm}$ roots from each other in a consistent way. However, by setting the imaginary part to be successively smaller and smaller, we may identify the convergence point for zero imaginary part. Furthermore, on setting the imaginary part to the same magnitude as the machine precision, we allow ourselves to maintain the conditions described above, but to have no noticeable effect on the precision of the results. It therefore follows that the twin cascade resonances described in this paper correspond to genuine trapped modes with real frequency. From here on we use the notation $\Omega = \Omega_r + \mathrm{i}\Omega_i$ to represent the real and imaginary parts of the frequency.

In practice, due to the non-dimensionalization used here, that is using the flow speed, U_∞^*, rather than the sound speed, a_∞^*, as our reference speed, and the fact that a non-zero vorticity wave amplitude can exist only for $M > 0$, the problem becomes singular for $M = 0$, and we must use a small but finite M to check zero flow results. In this case we use a small but finite flow speed, typically in the range $0.01 \leqslant M \leqslant 0.1$ and retain some finite negative imaginary part of Ω, depending on the flow speed. Koch (1983) found that for a cascade the imaginary part of the frequency is typically around 3% of the size of the real part for $M = 0.1$, and we used this as an initial estimate for finding our resonant frequencies.

In order to determine the values of Ω for which the matrix $\boldsymbol{Q}$ becomes singular, it is unfortunately not feasible to use the zero determinant condition, since it is quite possible, due to rounding error, to have matrices with very small determinants which are far from singular, and likewise to have matrices with numerically $O(1)$ determinants that are in fact singular. Instead, we adopt the most widely used alternative method of singular value decomposition (SVD), see for instance Golub & Van Loan (1996) or Stoer & Bulirsch (1980). Essentially, SVD factorizes a matrix $\boldsymbol{A}$ into a product of two orthogonal matrices, $\boldsymbol{U}$ and $\boldsymbol{V}$, and a real diagonal matrix, $\boldsymbol{D}$,

the entries of which are the 'singular values' of $\boldsymbol{A}$, and the condition number of $\boldsymbol{A}$ is defined as the ratio of the largest and smallest singular values. Formally, a matrix is singular if its condition number is infinity, but for numerical purposes can be taken to be singular if its condition number is greater than the reciprocal of 'machine precision' (typically around 10^{-15}.) Even here, it is often quite difficult, due to truncation and round-off errors earlier in the computation, to achieve this level of singularity, and a more useful test of whether a matrix is singular is to determine whether its condition number is greater than the reciprocal of some norm of the expected error in the matrix. For example, if the entries of the matrix can be calculated to a precision of 10^{-4}, then the matrix can be considered singular if its condition number is greater than 10000. For our purposes, this is a most important point, as each element of our coupling matrices is the result not only of a large number of algebraic operations, but also of an infinite product calculation in determining the Wiener–Hopf factors, and therefore is highly unlikely to be accurate to machine precision.

It is clear from the above comments that the formal and rigorous proof of the existence of resonant states in our system cannot be achieved numerically. However, we suggest that if the matrix is close to singularity at some set of parameter values, then it indicates that even if the system does not have a perfect resonance at this point it is at least very close to resonance, and may resonate either by detailed fine tuning of some parameters, or by inclusion of some additional small feature not considered in this model. In other words, the prediction of most practical interest is to determine ranges of parameters for which the system is susceptible to the excitation of acoustic resonance. From now on we shall therefore use the word 'resonance' in conjunction with acoustic modes to denote a situation where the numerical system displays behaviour which is significantly closer to singularity than that found over the majority of the rest of the parameter range, and this distinction will become more apparent in the next section, where we show the results of the numerical investigation. Despite our reliance on the condition number, we will also check that the matrix determinant is genuinely small at resonance, in order to eliminate those situations where the condition number is large due not to a zero eigenvalue but due to one very large eigenvalue.

6. Results

6.1. *Preliminary results*

As a way of checking most of our numerical and analytical routines, we look for resonances of the *single* cascade systems investigated analytically by Koch (1983) and Peake (1993) and experimentally by Parker (1966). By setting the amplitude of the vorticity wave incident on the stator to zero in our analysis, we may look for resonances of the pressure field, which should correspond exactly to the Parker modes. Parker studied an unstaggered single cascade system and found, by experiment (Parker 1966) and numerical (Parker 1967) means, four modes: the α and β modes with $\sigma = \pi$, and the γ and δ modes with $\sigma = 2\pi$. Our calculations of the resonant frequencies of this system are given in table 1, and clearly show excellent agreement with the original findings.

6.2. *General effects*

We start with a sample configuration used by Legerton (1992) to generate Figure 5.30 therein, and look at the effects of finite blade chord, matrix truncation number and imaginary part of frequency. He performed wind tunnel experiments on a twin annular

Mode	Parker Exp.	Parker Num.	Wiener–Hopf
α	0.92	0.94	0.929
β	0.494	0.52	0.497
γ	0.747	0.753	0.745
δ	0.582	0.575	0.573

TABLE 1. Comparison of Wiener–Hopf resonance frequency calculation with those of Parker (1966, 1967).

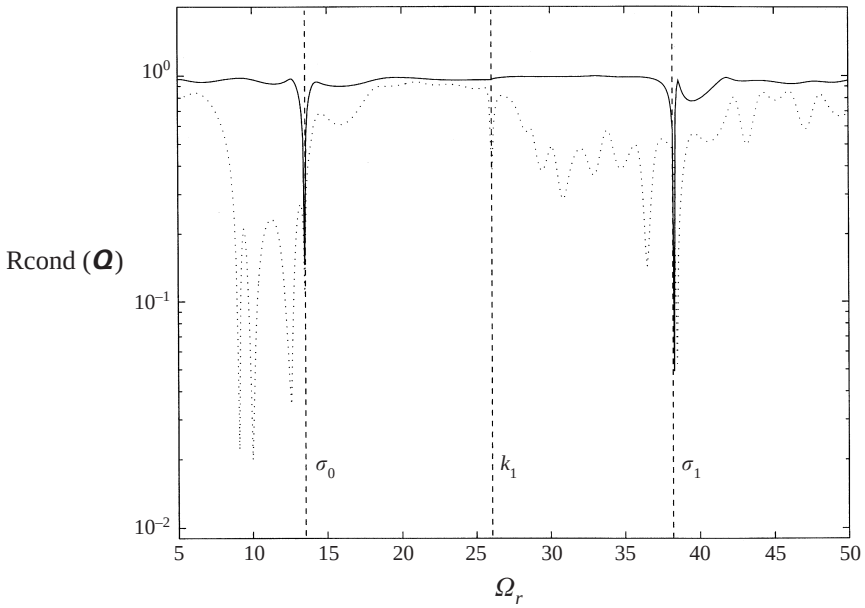

FIGURE 3. Reciprocal condition number, Rcond($\boldsymbol{Q}$), against real part of frequency, Ω_r, for semi-infinite (solid) and finite (dotted) blades, showing the frequencies at which the σ_0, k_1 and σ_1 modes cut on.

rig, with 15 thick, unstaggered blades on each row, inter-blade-row gap of 35 mm, rotor chord 70 mm, stator chord 40 mm and flow speeds from 0 to around 50 m s^{-1}. This gives non-dimensional parameters $c = 1.143$, $\hat{c} = 2$, $g = 1$ and $\Delta = 1.216$ (where Δ is the non-dimensional leading-edge separation). Since our present method is not really suitable for zero stagger (this is because Peake's 1992 calculations rely on splitting up the blade chords into portions which overlap with adjacent blades – an equivalent formulation with $d = 0$ could easily be derived), we use small but finite stagger, typically $\alpha = 0.45\pi$. Similarly, we use $M = 0.1$ in most cases for our flow Mach number, and look at the azimuthal mode number $m = 4$, giving an inter-blade phase angle of $\sigma = 8\pi/15$. All results in this section use these parameters, or small changes to them which are noted at relevant points in the text. Throughout, we show Ω as the independent variable, although it should be noted that in many cases $M\Omega$ is a more appropriate measure of the reduced frequency, due to our non-dimensionalization. However, we shall retain the use of Ω on its own since later we shall go on to look at how changes in Mach number can cause resonances to appear, and consequently need to have different Mach number lines on the same graph.

We first look at twin semi-infinite blade and twin finite blade systems, as the comparison between these two situations will be useful later on in deducing the relevant driving mechanisms for the resonances. Figure 3 shows the general type of situation encountered and shows the difference in behaviour between the finite blade and semi-infinite blade cases.

For the semi-infinite blade case, shown as a solid line, there are two distinct resonance points, at $\Omega \approx 13.5$ and $\Omega \approx 38$, corresponding to the frequencies at which the $\sigma_0^{\pm}$ and $\sigma_1^{\pm}$ modes cut-on respectively. These may be shown to be the Tyler–Sofrin 'spinning modes' (Tyler & Sofrin 1962), where a mode that is just cut-on propagates parallel to the blade face. It will be shown later in this section that the minimum of the reciprocal condition number may be forced as low as required within the bounds of numerical error, simply by increasing the frequency resolution. However, for the finite blade case (dotted line), things are somewhat different; we found that although the finite system seems to exhibit some excitation close to these Tyler–Sofrin mode resonance points, the finite chord effects 'detune' the resonance slightly. The other excitations seen in figure 3 at $\Omega \approx 9.2$, 10.0, 12.6 and 38.5 are associated with the finite blade chord and will be considered in more detail later. We emphasize again that the imaginary part of Ω can be forced as close to zero as required, and this means that the twin cascade resonances found in this paper correspond to genuine trapped modes.

6.3. *Finite blade effects*

We now go on to show some more details of the system's behaviour, starting with the effects of finite blade chord on the resonance points. We find a range of resonance types, each associated with different aspects of the system. First of all there are the Tyler–Sofrin spinning mode resonances, of the form seen above, which are associated with the gap between the blade rows and are relatively unaffected by changes in blade chord. Then there are other resonance-like events, the occurrence of which displays a strong dependence on which of the finite or infinite blade chord models is used. This variation in behaviour can be clearly seen in figure 3, where we see that for a range of frequencies there exist slightly different resonant (or near-resonant) frequencies, depending on whether the blades are finite or not.

Careful examination of all our data revealed that for the twin semi-infinite blade cases, resonances may only occur at frequencies at which one of the $\sigma_n^{\pm}$ modes changes from cut-on to cut-off in the gap, i.e. $\sigma_n^+ = \sigma_n^-$ for some n. At first sight this may seem obvious, for this corresponds to the case where there is a standing wave in the gap between the blade rows – a left-travelling σ_n^+ wave and an equal right-travelling σ_n^- wave. However, this is misleading, as the coordinates are aligned along the blade chords, not in blade face coordinates, and hence the y dependence of these waves is slightly different. Evaluation of the wavenumbers in the blade face coordinates $\tilde{x}$ and $\tilde{y}$, parallel and perpendicular to the blade row face shows that the resonant modes are just the Tyler–Sofrin spinning modes, which travel up and down the gap in the $\tilde{y}$-direction, with no group velocity component perpendicular to the blade row face. To calculate these frequencies we simply need to solve the equation $\sigma_n^+ = \sigma_n^-$ for Ω. Substituting the expressions for $\sigma_n^{\pm}$ (2.14) and solving for Ω, we get

$$\Omega = \pm \frac{\cos\alpha}{\Delta}(2n\pi - \sigma)\left[1 \pm \left\{1 + \left(\frac{1}{M^2} - 1\right)(1 + \tan^2\alpha)\right\}^{1/2}\right], \tag{6.1}$$

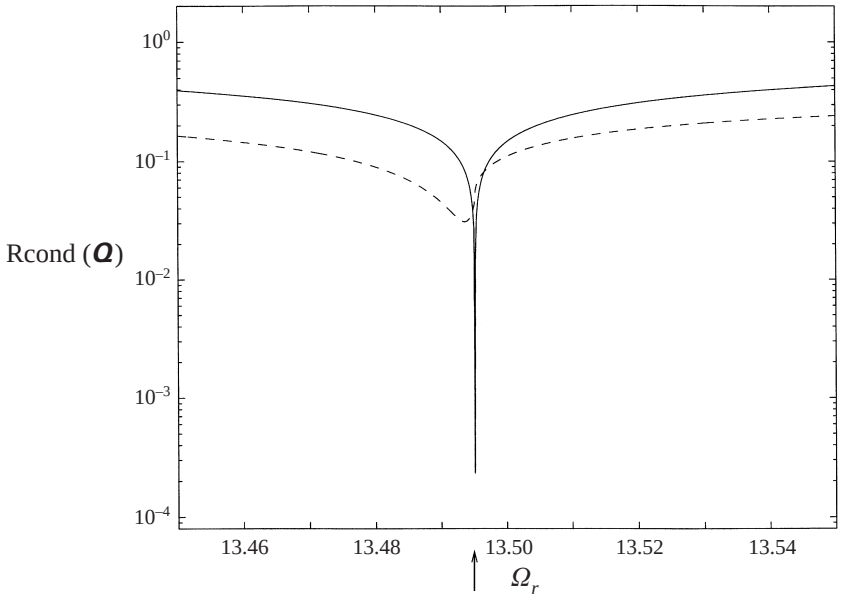

FIGURE 4. Reciprocal condition number, Rcond(**Q**), against real part of frequency, Ω_r, for semi-infinite (solid) and finite (dashed) blades. The arrow indicates where σ_0 is first cut on.

where the $\pm$ signs are unrelated, giving four possible frequencies, only two of which will be positive.

Figure 4 shows a higher-resolution view of the Tyler–Sofrin-type resonance point at $\Omega = 13.5$, for the semi-infinite blade case, showing that the reciprocal condition number has a sharp cusp as one refines the frequency step resolution. This cusp may be forced even lower by greater increases in frequency resolution, but introduction of finite blades damps out this resonance and 'smooths off' the cusp. This could be due to the interaction of the $k_0^{\pm}$ duct modes with the rotor leading and stator trailing edges, causing energy to be scattered back into the inter-blade-row gap, and cancelling with some of the waves there, or could be due to the stator trailing-edge vorticity wave extracting energy from the resonant field. The main point to note is that a Tyler–Sofrin-type spinning mode resonance exists for twin semi-infinite blade systems, but introduction of finite blades detunes this Tyler–Sofrin resonance, leaving just a small range of the reduced frequency where the system can be regarded as in a more exited state than elsewhere.

Figures 5 and 6 show the relative effects of taking either the stator (figure 5) or rotor (figure 6) to have a semi-infinite chord, with the other blade row finite. We can clearly see that introduction of a semi-infinite stator changes the behaviour quite significantly at high frequencies, but has less of an effect at low frequency, although both cases have two Tyler–Sofrin-type excitations at $\Omega \approx 13.5$ and $\Omega \approx 38$. In the twin finite case we have three finite-chord-type resonance points at low frequencies, $\Omega \approx 9$, 10 and 12.5, and one at higher frequency, $\Omega \approx 36$, whereas with a semi-infinite stator, we have only two finite-chord resonance points at low frequencies, $\Omega \approx 10$ and 11.5. The major effect of neglecting the stator trailing edges then is to remove high-frequency resonances, indicating that these are resonances of the stator, possibly driven by the rotor vorticity wave.

In contrast, figure 6 shows that assuming a semi-infinite rotor chord has relatively

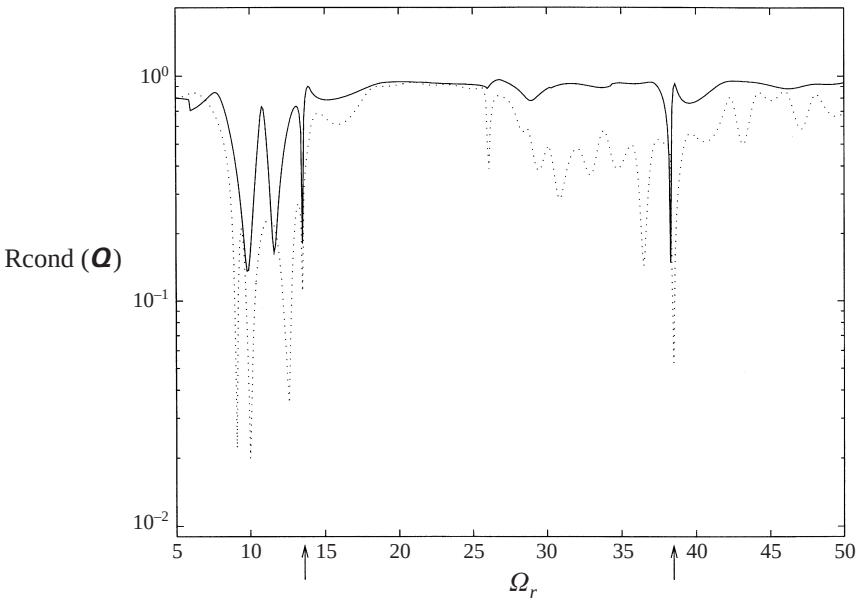

FIGURE 5. Reciprocal condition number, Rcond($\boldsymbol{Q}$), against real part of frequency, Ω_r, for finite–infinite (solid) and finite–finite (dotted) blades. The arrows indicate where σ_0 and then σ_1 are first cut on.

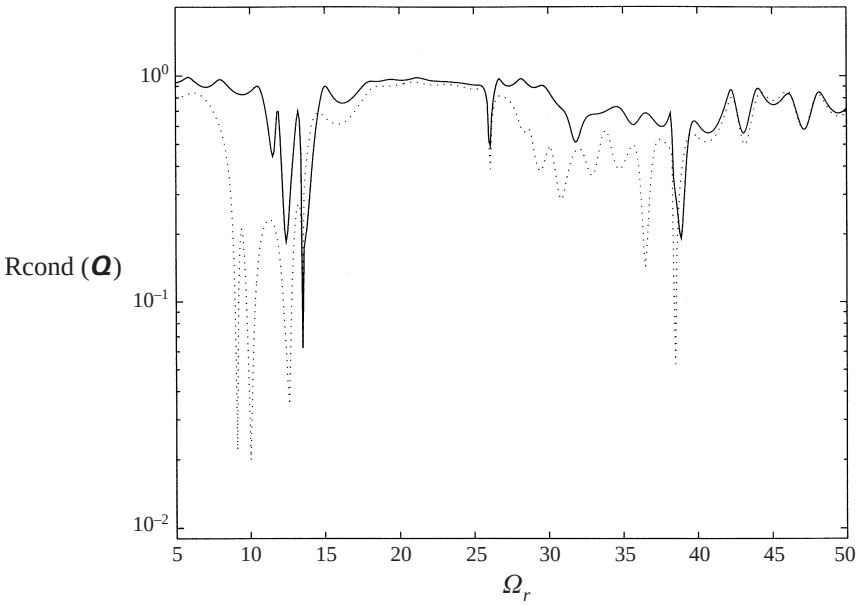

FIGURE 6. Reciprocal condition number, Rcond($\boldsymbol{Q}$), against real part of frequency, Ω_r, for infinite–finite (solid) and finite–finite (dotted) blades.

little effect at high frequencies, but more at low frequencies. We have the same three finite-chord resonances as above, at $\Omega \approx 9$, 10 and 12.5, but all are destroyed by the removal of rotor leading-edge effects. This would appear to be due to the fact that for the high-frequency resonance at $\Omega \approx 38$ there are propagating radiation modes

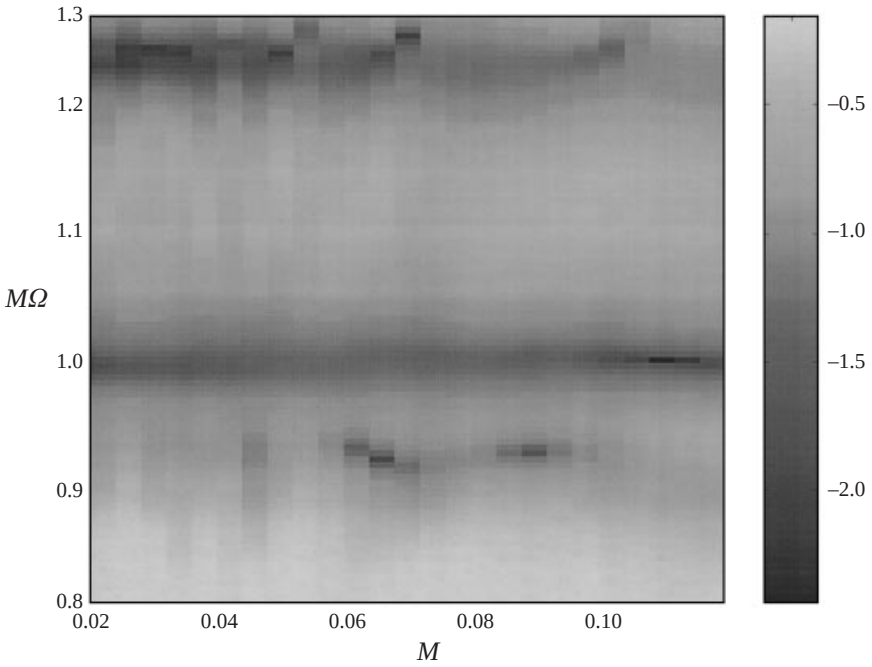

FIGURE 7. Surface plot of the logarithm of the reciprocal condition number, $\log_{10}\mathrm{Rcond}(\boldsymbol{Q})$, as a function of mean flow Mach number, M, and scaled frequency, $M\Omega$.

in the gap, giving a mechanism for the generation of vorticity waves from the rotor trailing edge. At low frequencies, however, all the radiation modes are cut-off in the gap, so that the only way of producing vorticity waves is by downstream-travelling duct modes incident on the rotor trailing edge. Obviously this can only happen with a finite-chord rotor, since this is the only way that a non-zero field can be trapped in the rotor. In these low-frequency resonance cases, the rotor seems to play a relatively unimportant role, other than the requirement that it be finite; we found that changing the rotor chord length slightly merely alters the resonant frequency, whereas introducing a semi-infinite rotor destroys the resonance point completely.

In figure 7 we see that small changes in the mean flow Mach number in this case can have a significant effect on the resonance behaviour. Note that the vertical axis shows the quantity $M\Omega$, rather than Ω now, as this quantity remains relatively unchanged as M varies, allowing easier visualization of the features on the graph. We can see that there are two regions of reasonably robust excitation, at $M\Omega \approx 1.0$ and $M\Omega \approx 1.26$, that persist throughout the range of M considered, with sharp resonances at certain points along the range, for example for $M\Omega \approx 1.26$, resonances at $M \approx 0.03$, 0.05 and 0.07. Isolated resonances exist at other points. From this graph we see that the non-resonant excitation points may be forced into resonant conditions by changes in the flow speed. In fact, we found that this resonance 'tuning' may be done by varying any one of the system parameters, such as blade chord, but for our purposes changing the Mach number seems to be more physically realistic. For example, at $M \approx 0.1$, there is a resonance point for $M\Omega \approx 1.01$, but at no lower frequencies, whereas at $M \approx 0.09$ there is a new resonance point at $M\Omega \approx 0.92$, and the reciprocal condition number at $M\Omega = 1.01$ is not as low as it is at $M = 0.1$. Further refinements in resolution reveal the new resonance to be at $M = 0.08742$, $M\Omega = 0.9267$, with a

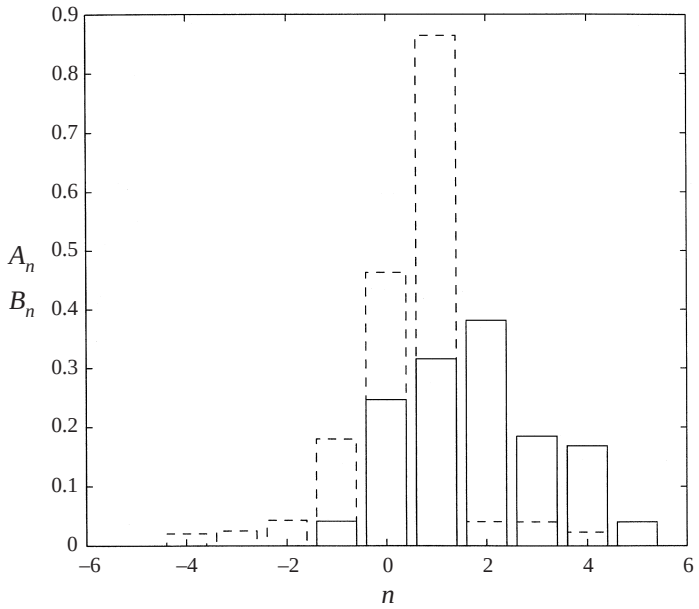

FIGURE 8. Relative mode amplitudes, A_n and B_n for $\Omega_r = 34.59$. The left-travelling wave mode amplitudes, shown in dashed lines, represent the magnitude of the A_n, $-4 \leqslant n \leqslant 4$, and the right-travelling waves, shown in solid lines, denote the magnitude of the B_n, $-4 \leqslant n \leqslant 5$, where B_5 represents the vorticity wave amplitude.

reciprocal condition number of 6.4×10^{-5}. This value may be forced even lower by further increases in Mach number/frequency space resolution.

These low-frequency resonances, at $M\Omega \approx 0.92$, 1.01 and 1.26, occur under conditions where all modes except the $k_0^{\pm}$ duct modes are cut-off, and seem to correspond to Parker-mode-like resonances of the stator, excited by the incident vorticity wave shed by the rotor. Although true Parker modes require a phase angle of $n\pi$ between blades, this is only necessary to provide a resonant mode at all geometry and flow conditions, as imposing this angle ensures that the zero normal velocity condition on the blade is satisfied. For other phase angles we can still have a resonant mode, but may need certain combinations of blade row geometry, mean flow etc. to satisfy the normal velocity boundary conditions. This Parker-mode-like behaviour is further confirmed by determining the Parker frequency (with phase angle $\sigma = \pi$, as for a Parker α or β mode) for the stator in isolation, as in § 6.1. We found a resonance point with frequency $\Omega_r = 18.6$, giving good agreement with our calculated Parker α-mode frequency for the stator, $\Omega_r = 17.9$, indicating that this is probably the physical mechanism present, with a small change due to the vorticity wave incident on the stator. The reason for this would appear to be that since all the radiation modes are cut off, the vorticity wave in the gap must be caused by downstream-travelling duct modes incident on the rotor trailing edge. Since there is no energy entering the system from upstream of the rotor, these downstream-travelling duct modes can only arise due to the incidence of upstream-travelling duct modes on the rotor leading-edge region. The resonance thus takes the form of re-reflecting $k_0^{\pm}$ duct modes in the rotor generating vorticity waves to drive a Parker-mode-like resonance of the stator.

We repeated the above investigation for higher-frequency modes, where there exist several cut-on modes; we found that the excitation at $\Omega \approx 38$ can be 'tuned' into

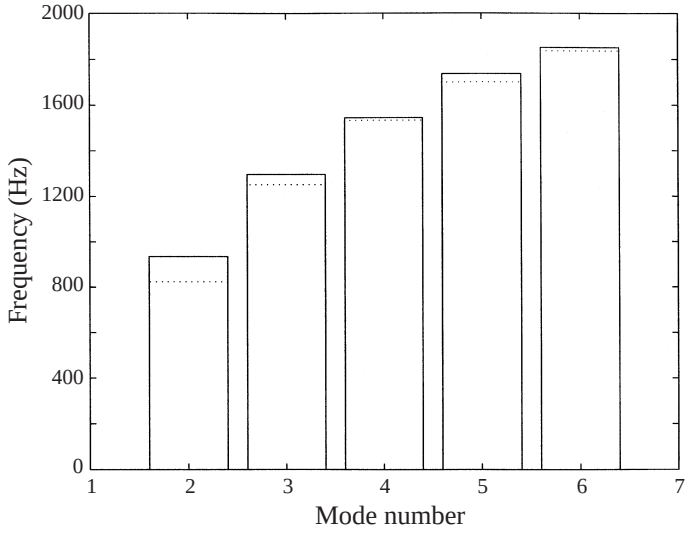

FIGURE 9. Resonance frequencies for the experimental setup of Legerton (1992) (solid lines) and Wiener–Hopf theory (dotted).

a resonance by increasing the mean flow Mach number to $M = 0.1067$, giving a sharp resonance point at $\Omega_r = 34.59$, with $\mathrm{Rcond}(\boldsymbol{Q}) \approx 2 \times 10^{-5}$. The resonance field here does not appear to have a simple form, and involves both the cut-on σ_0^+ and σ_0^- radiation modes, allowing energy to be transmitted between the blade rows. At this resonant point, we may solve for the eigenvector corresponding to the zero eigenvalue and hence find the modeshape. Figure 8 shows the amplitudes A_n and B_n of the radiation modes in the gap, for $N = 4$. In this case, although only the $\sigma_0^{\pm}$ modes are cut-on, the amplitudes of many of the cut-off modes are still relatively high. We see that the vorticity wave amplitude is much smaller than the radiation mode amplitudes, indicating that in this high-frequency case it is probably the pressure wave reflection between the blade rows that is the dominant source of the resonance, rather than the vorticity wave driving a Parker mode of the stator as in the low-frequency resonance cases discussed above.

6.4. *Comparison with experiment*

To enable comparison with other results, bearing in mind the above comments regarding resonances not occurring at all flow conditions, we use graphs of the form shown in figure 7, thus giving an instant picture of which flow conditions are likely to be close to a resonance point. We now turn to the experimental results of Legerton (1992) and present some theoretical predictions calculated from our analysis for comparison with his experimental data.

Legerton's experimental setup consisted of two stationary annular blade rows, each with 15 fairly thick unstaggered blades, in a wind tunnel at speeds around $50\,\mathrm{m\,s^{-1}}$. The experimental data were taken from the $g^* = 35\,\mathrm{mm}$ graph of Figure 5.30 in Legerton (1992), and comparison with our Wiener–Hopf predictions are shown in figure 9, for five different circumferential mode numbers. For the Wiener–Hopf theory predictions we took the lowest-frequency resonance point we could find that occurred reasonably consistently across the flow speed range considered, so for the case in figure 7 we took $M\Omega = 1.01$, and not the lower isolated frequencies of around $M\Omega = 0.92$ that are clearly present in that figure. The Wiener–Hopf theory shows

excellent agreement with the experimental measurements, with errors of less than 4% for all but the lowest mode number, where the prediction is around 12% too low. We expect the lowest mode, with the longest azimuthal wavelength, to be most affected by our assumption of small annulus curvature, but even so the agreement is still reasonable at this low frequency.

The differences between our Wiener–Hopf predictions and the experimental results could be quite easily accounted for by the thickness of the blades, the blockage ratio being around 9% for the mid-radius station we took for our cascade unwrapping, and by the large curvature of the annulus; Legerton's annulus has inner and outer radii of 75 mm and 127 mm respectively, and for our calculations we simply took the average of $R = 101.6$ mm as our reference radius. Related to this, we should mention that many of the resonances shown here are at points close to, but not actually at, a cut-on/cut-off condition, which has been shown Majumdar & Peake (1996) to be a situation where three-dimensional effects become important. Even so, the good agreement between the cascade theory and annular experiment gives considerable confidence in the validity of the approach adopted in this paper.

7. Conclusions

We have found the exact solution to the problem of acoustic scattering in a system consisting of two stationary, finite-chord blade rows in non-zero axial flow, using the Wiener–Hopf technique. A number of resonant states have been identified, and it is again emphasized that these occur for frequencies with a (to the level of numerical accuracy) zero imaginary part, and therefore correspond to genuine trapped modes. This is in contrast to the single cascade with axial flow, in which Koch (1983) showed that the Parker resonances are damped.

One of the most important features of our system is the fact that the blade chords are genuinely finite, and as we saw in figures 3, 5 and 6, this can have different effects depending on the frequency. For the twin semi-infinite blade systems, the only resonances are seen to be the Tyler–Sofrin spinning modes, at the points where a radiation mode changes from cut-on to cut-off in the inter-blade-row gap. However, these resonances are 'smoothed off' by the introduction of finite blade chord effects, to give a relatively small reciprocal condition number which cannot be forced lower by increases in frequency step resolution. Even so, the system can then be regarded as being close to an excited state, and experience showed that it can often be 'tuned' into a sharp resonance by changes in the flow or geometry parameters.

As well as these cut-on/cut-off resonances, however, the genuine finite-chord system has been seen to possess resonant modes of its own, akin to a Parker-mode resonance of the stator, the driving mechanism of which depends on the frequency. At low frequencies, where all radiation modes are cut-off, the sole resonance mechanism appears to be the trapped duct waves in the finite-chord rotor generating vorticity waves to drive a stator Parker mode. This is demonstrated by the fact that using a semi-infinite rotor in our calculations eliminates the resonance. At higher frequencies, the Parker-mode-type resonance is driven by either the vorticity wave or by the (now cut-on) downstream-propagating pressure waves from the rotor. In this case, the cut-on radiation modes in the gap provide a means of energy transmission downstream of the rotor, and we find that we do not need a finite-chord rotor to obtain these resonances.

Clearly, finite-chord effects have a large role to play in determining the possible resonances of a twin cascade system. Although resonances may be excited with twin

semi-infinite cascades, the reflection effects introduced by using, for example, a finite-chord stator, can generate more system excitation than would be seen otherwise, even if we are not actually at a resonance condition. As shown in figure 7, small changes in mean flow speed or other parameters may shift the system into a resonant state at some distinct frequency. Fortunately, there would appear to be only certain combinations of parameters that give a resonance; for any given situation, there is not necessarily a resonant frequency. The resonant conditions thus define a path in parameter space for the system. If the system state lies on this path there is at least one resonant frequency of the system, and for states close to the path, the system may be regarded as close to resonance and very sensitive to changes in flow or geometry parameters. The results presented here for the resonant frequencies can be combined with predictions of the vortex-shedding frequencies of the blade rows, in order to predict the possible onset of acoustic resonance. In practical systems, the rotor will of course rotate relative to the stator, and in Part 2 we will show how the analysis presented here can be extended to include non-zero relative rotation.

The authors are grateful for financial support provided by EPSRC and Rolls-Royce plc, and to Dr A. B. Parry for helpful conversations.

Appendix A. Stator transmission matrices

In this Appendix we simply state expressions for the various duct-mode reflection matrices described in § 2.2.

The reflection matrix $R_{pm}^{\mathscr{D}\mathscr{D}}$ is very similar to that given in Peake (1993), and may be written as

$$R_{pm}^{\mathscr{D}\mathscr{D}} = \frac{\mathrm{i}\epsilon_m \mathrm{e}^{-\mathrm{i}k_p^-(c-d)}(1-\mathrm{e}^{\mathrm{i}(\sigma+k_m^+d+m\pi)})(1-\mathrm{e}^{-\mathrm{i}(\sigma+k_p^-d+p\pi)})(k_p^- - \Omega)}{s\left(k_m^+\beta^2 + M^2\Omega\right)\mathscr{K}^+\left(k_m^+\right)\left(k_p^- - k_m^+\right)\mathscr{K}^-\left(k_p^-\right)}, \tag{A 1}$$

where as in Peake (1993), $\epsilon_m = 1$ for $m \neq 0$ and $\epsilon_0 = \frac{1}{2}$, but we have an extra $\exp(\mathrm{i}k_p^- d - \mathrm{i}k_p^- c)$ term due to our different length scale used for non-dimensionalization. Likewise, two transmission matrices may be taken from equation (3.18) of Peake (1993) as

$$T_{pm}^{\mathscr{D}\mathscr{D}} = -\frac{\mathrm{i}\epsilon_m \mathrm{e}^{\mathrm{i}(k_p^+c - k_m^-d)}(1-\mathrm{e}^{\mathrm{i}(\sigma+k_m^-d+m\pi)})(1-\mathrm{e}^{-\mathrm{i}(\sigma+k_p^+d+p\pi)})\left(k_p^+ - \Omega\right)}{s\left(M^2\Omega + \beta^2 k_m^-\right)\left(k_m^- - k_p^+\right)\mathscr{K}^+\left(k_p^+\right)\mathscr{K}^-\left(k_m^-\right)}, \tag{A 2}$$

and

$$T_m^{\mathscr{V}\mathscr{D}} = \frac{\epsilon_m \mathrm{e}^{-\mathrm{i}k_m^- d}(1-\mathrm{e}^{\mathrm{i}(\sigma+k_m^-d+m\pi)})\mathscr{K}^-(\Omega)}{s(M^2\Omega + \beta^2 k_m^-)\mathscr{K}^-(k_m^-)(k_m^- - \Omega)}. \tag{A 3}$$

Further consideration of equation (3.18) of Peake (1993) allows us to write down the equivalent pressure matrix as

$$T_{pm}^{\mathscr{P}\mathscr{D}} = -\frac{\mathrm{i}\epsilon_m \mu_p^- \mathrm{e}^{-\mathrm{i}k_m^- d}\mathscr{K}^-(\sigma_p^-)(1-\mathrm{e}^{\mathrm{i}(\sigma+k_m^-d+m\pi)})}{s\left(M^2\Omega + \beta^2 k_m^-\right)\mathscr{K}^-\left(k_m^-\right)\left(k_m^- - \sigma_p^-\right)}. \tag{A 4}$$

To find $T_{pm}^{\mathscr{D}\mathscr{P}}$ we must return to equation (3.23) of Peake (1993), where closing the integration contour in the upper half-plane gives the expression

$$T_{pm}^{\mathscr{D}\mathscr{P}} = -\frac{\mathscr{K}^+\left(\sigma_m^+\right)}{2\left(\sigma_m^+ - \Omega\right)} \times Res_{\sigma_m^+}^1 \times \frac{(k_p^+ - \Omega)(1-\mathrm{e}^{-\mathrm{i}(\sigma+k_p^+d+p\pi)})\mathrm{e}^{\mathrm{i}k_p^+c}}{\left(\sigma_m^+ - k_m^+\right)\mathscr{K}^+\left(k_p^+\right)}, \tag{A 5}$$

where $Res_{\sigma_m^+}^1$ is defined in § 2.1.

Appendix B. Rotor transmission matrices

In this Appendix we present the expressions for the coupling matrices used in the rotor scattering calculations. We may take two of the matrices straight from Peake (1993) as

$$\hat{T}^{\mathscr{D}\mathscr{D}}_{pm} = -\frac{\mathrm{i}\epsilon_m \mathrm{e}^{\mathrm{i}(k_p^+\hat{c}-k_m^-d)}(1-\mathrm{e}^{\mathrm{i}(\sigma+k_m^-d+m\pi)})(1-\mathrm{e}^{-\mathrm{i}(\sigma+k_p^+d+p\pi)})(k_p^+-\Omega)}{s\left(M^2\Omega+\beta^2k_m^-\right)\left(k_m^--k_p^+\right)\mathscr{K}^+\left(k_p^+\right)\mathscr{K}^-\left(k_m^-\right)}, \tag{B 1}$$

and

$$\hat{R}^{\mathscr{D}\mathscr{D}}_{pm} = \frac{\mathrm{i}\epsilon_m \mathrm{e}^{\mathrm{i}k_p^-(\hat{c}-d)}(1-\mathrm{e}^{\mathrm{i}(\sigma+k_m^+d+m\pi)})(1-\mathrm{e}^{-\mathrm{i}(\sigma+k_p^-d+p\pi)})\left(k_m^+-\Omega\right)}{s\left(M^2\Omega+\beta^2k_m^+\right)\left(k_p^--k_m^+\right)\mathscr{K}^+\left(k_m^+\right)\mathscr{K}^-\left(k_p^-\right)}. \tag{B 2}$$

Here the quantity $\hat{c}$ corresponds to the normalized rotor blade chord, which can differ from the normalized stator chord c.

Inspection of equation (3.44) of Peake (1993) reveals that closing the inversion contour in the lower half-plane gives pole contributions at $k=\Omega$ and at $k=\sigma_m^-$, thus yielding the vorticity and pressure wave amplitudes from the duct mode scattering at the trailing edge. After some manipulation we may write these down in the forms

$$\hat{T}^{\mathscr{D}\mathscr{V}}_{m} = \frac{\mathrm{e}^{-\mathrm{i}k_m^-\hat{c}}(1-\mathrm{e}^{-\mathrm{i}(\sigma+k_m^-d+m\pi)})\mathscr{K}^-(\Omega)}{2\mathscr{K}^-\left(k_m^-\right)}, \tag{B 3}$$

and

$$\hat{T}^{\mathscr{D}\mathscr{P}}_{pm} = \frac{\hat{\mathscr{K}}^-\left(\sigma_m^-\right)}{2\left(\Omega-\sigma_m^-\right)} \times Res^2_{\sigma_m^-} \times \frac{\mathrm{e}^{-\mathrm{i}k_p^-\hat{c}}(k_p^--\Omega)(1-\mathrm{e}^{-\mathrm{i}(\sigma+k_p^-d+p\pi)})}{2\mathscr{K}^-\left(k_p^-\right)\left(k_p^--\sigma_m^-\right)}. \tag{B 4}$$

The only remaining unknown is now $\hat{T}^{\mathscr{P}\mathscr{D}}_{pm}$, which we can obtain by taking equation (3.2) from Peake (1993) and, after rewriting the kernel function as in equation (3.14) of Peake (1993), closing the inversion contour in the upper half-plane. We pick up contributions from the poles at $k=k_m^+$, and eventually may write the transmission matrix as

$$\hat{T}^{\mathscr{P}\mathscr{D}}_{pm} = \frac{\mathrm{i}\epsilon_m\lambda_p^+\mathrm{e}^{-\mathrm{i}k_m^+d}\mathscr{K}^+(\sigma_p^+)(1-\mathrm{e}^{\mathrm{i}(\sigma+k_m^+d+m\pi)})}{s\left(M^2\Omega+\beta^2k_m^+\right)\mathscr{K}^+\left(k_m^+\right)\left(k_m^+-\sigma_p^+\right)}. \tag{B 5}$$

REFERENCES

Evans, D. V., Levitin, M. & Vassiliev, D. 1994 Existence theorems for trapped modes. *J. Fluid Mech.* **261**, 21–31.

Evans, D. V. & Linton, C. M. 1991 Trapped modes in open channels. *J. Fluid Mech.* **225**, 153–175.

Evans, D. V. & Linton, C. M. 1994 Acoustic resonance in ducts. *J. Sound Vib.* **173**, 85–94.

Golub, G. H. & Van Loan, C. F. 1996 *Matrix Computations.* Johns Hopkins University Press.

Koch, W. 1971 On the transmission of sound waves through a blade row. *J. Sound Vib.* **18**, 111–128.

Koch, W. 1983 Resonant acoustic frequencies of flat plate cascades. *J. Sound Vib.* **88**, 2, 233–242.

Legerton, M. L. 1992 Flow induced acoustic resonances. PhD thesis, University of Wales, Swansea.

Majumdar, S. J. & Peake, N. 1996 Three-dimensional effects in cascade-gust interaction. *Wave Motion* **23**, 4, 321–337.

Parker, R. 1966 Resonance effects in wake shedding from parallel plates: some experimental observations. *J. Sound Vib.* **4**, 1, 62–72.

Parker, R. 1967 Resonance effects in wake shedding from parallel plates: calculation of resonant frequencies. *J. Sound Vib.* **5**, 330–343.

Parker, R. & Stoneman, S. A. T. 1989 The excitation and consequences of acoustic resonances in enclosed fluid flow around solid bodies. *Proc. Inst. Mech. Engrs* **203**, 9–19.

Peake, N. 1992 The interaction between a high-frequency gust and a blade row. *J. Fluid Mech.* **241**, 261–289.

Peake, N. 1993 The scattering of vorticity waves by an infinite cascade of flat plates in subsonic flow. *Wave Motion* **18**, 255–271.

Stoer, J. & Bulirsch, R. 1980 *Introduction to Numerical Analysis*. Springer.

Tyler, J. M. & Sofrin, T. G. 1962 Axial flow compressor noise studies. *SAE Trans.* **70**, 309–332.

Woodley, B. M. & Peake, N. 1997*a* Global linear instability of thin aerofoil wakes. *J. Fluid Mech.* **339**, 239–260.

Woodley, B. M. & Peake, N. 1997*b* Vortex shedding from a cascade of aerofoils. *AIAA Paper* 97-1814.

Woodley, B. M. & Peake, N. 1999 Resonant acoustic frequencies of a tandem cascade. Part 2. Rotating blade rows. *J. Fluid Mech.* **393**, 241–256.